Intraseasonal modulation of spring-strong wind events associated with convection in northeastern Argentina.

Federico Otero [1 4]

Mariano S. Alvarez, Paola Salio and Carolina Vera [2 3 4]

[1] **Instituto Argentino de Nivología, Glaciología y Ciencias Ambientales**

[2] **Centro de Investigaciones del Mar y la Atmosfera CIMA – CONICET - UBA**

[3] **Departamento de Ciencias de la Atmósfera y los Océanos, FCEyN, UBA**

[4] **Instituto Franco-Argentino sobre Estudios de Clima y sus Impactos UMI IFAECI 3351-CNRS-CONICET-UBA**

Manuscript submitted to

International Journal of Climatology

April 2018

Corresponding author address: Federico Otero. Instituto Argentino de Nivología, Glaciología y Ciencias Ambientales. (IANIGLA) CCT Mendoza - CONICET. Av. Ruiz Leal s/n., Parque Gral. San Martín, (5500) Mendoza, Argentina. Email: fotero@mendoza-conicet.gob.ar

Abstract

The relationship between intraseasonal variability (IS, 10-90 days) and days which registered **C**onvection-associated **S**trong **S**urface **W**ind **E**vents (CSSWE) over Northeastern Argentina (NEA) was studied. The climatological behavior of these strong wind events showed a higher duration and occurrence in austral spring. CSSWE were categorized as a function of the wet and dry phases of the spring-**S**eason **I**ntra**S**easonal (spring-SIS) index, which describes the activity of the leading pattern of IS-filtered outgoing longwave radiation (IS-OLR) during that season in eastern South America. A modulation of the IS variability over localized and mesoscale phenomena as the CSSWE was found, showing significant peaks of wind variability in that time scale, and especially the submonthly time scale. The CSSWE were categorized according to the phases of the spring-SIS pattern and most of them occurred before or during a wet phase, especially for the longer CSSWE. Moreover, the detection of CSSWE days during and before a dry phase was scarce. Rossby wave trains were observed to organize the circulation on intraseasonal time scales that configure regional cyclonic anomalies in such way which favors the development of CSSWE, promoting mid-level ascents over NEA and northerly advection of humidity to the region. Together with the composites of IS-OLR anomalies and the spectra of wind velocity, they support the fact

that the higher-frequency IS variability is the primary influence for the development of CSSWE.

Key words: *Surface winds, strong convective events, intraseasonal variability, Northeastern Argentina*

1. Introduction

The potential for convective development in Southeastern South America (SESA) has been the focus of numerous studies. Nesbitt et al. (2003) and Rasmussen et al. (2014), among others, observed that the La Plata Basin is one of the regions with the highest frequency of occurrence of mesoscale convective systems (MCSs). In fact, Zipser et al. (2006) showed that this is one of the regions where the strongest MCSs on Earth occur. Responsible for approximately 60% of the total precipitation (Liu, 2011), MCSs in the region are also associated with severe weather events (Silva Dias, 1999, Matsudo and Salio, 2011, Mezher et al. 2012, Rasmussen et al. 2014, among others). The South American Low-Level Jet (SALLJ) east of the Andes transports considerable heat and moisture from the Amazon basin southward into the central plains of SESA, providing the ideal environmental conditions for convective initiation (Marengo et al. 2002, 2004, Vera et al. 2006, among others included in the text). SALLJ shows an intensity peak especially in spring months. The occurrence of extreme SALLJ events during summertime is associated with the presence of dipole-like outgoing longwave radiation (OLR) anomalies between SESA and the South Atlantic Convergence Zone (SACZ) region (Berbery and Barros, 2002 and Liebmann et al. 2004).

The SACZ is the region of South America with the largest IS activity with periods between 10 and 90 days (Liebmann et al. 1999). Nogues-Paegle and Mo (1997) show that this variability is associated with a meridional see-saw pattern of dry and wet conditions over tropical and subtropical South America (TSA). This pattern is influenced by the larger-scale conditions, related to the Tropics at least partially with the Madden Julian Oscillation (MJO, Madden and Julian, 1994) (Liebmann et al. 2004, Carvalho et al. 2004, Alvarez et al. 2016, among others). The dipole phase associated with an enhanced SACZ is related with strong tropical convection over the central Pacific and dry conditions over the western Pacific and the Maritime Continent. Liebmann et al. (1999) show that the IS variability of the SACZ-SESA regions is related to the activity of Rossby wave trains extended along the South Pacific that develop persistent circulation conditions over the region. The variability source has been associated with either atmospheric internal variability (e.g. westerly jet weakening promoting blocking events or the development or hemispheric quasi-stationary waves) or by climate conditions forced by tropical convection variability (like that associated with MJO). Such wave trains induce in South America a strong SALLJ near 20 p S and a baroclinic zone further south, which both seem to in turn force the northerly flow and consequently intensify convection over SESA. On the other hand, the Rossby wave trains associated with an enhanced SACZ are similar but with opposite sign (Liebmann et al. 2004).

The leading pattern of IS variability in South America during the warm season (that is the period that roughly goes from October to April) has significant amplitude in two specific bands: one with periods between 10 and 30 days, which has the highest percentage of explained variance, and the other with periods between 30 and 90 days, which is associated with the MJO activity (Gonzalez and Vera, 2014). Moreover, the MJO strongly modulates heavy precipitation events over SACZ and SESA during summer, as well as surface temperature and associated circulation anomalies (Hirata and Grimm, 2016a). MJO influence on regional climate in South America was also detected in spring as well as in the other seasons, although with large seasonal variations (Alvarez et al. 2016).

There are evidences that extreme daily rainfall events in SESA are associated with intense convection over the region and its inhibition in the SACZ region (e.g. Liebmann et al. 2004 and Gonzalez et al. 2008). Similarly, Alvarez et al. (2014) found that the leading pattern of IS-Filtered OLR anomalies (FOLR) in South America during winter, spatially characterized by a monopole-like center over SESA, modulates the occurrence of extreme daily precipitation events, as well as the sequence of consecutive rainy days (wet spells). These events occur more frequently during the positive phase of the leading pattern, which is defined as when FOLR anomalies are negative within SESA. On the other hand, Salio et al. (2007) show that convective activity in SESA is significantly modulated by synoptic-scale waves. Since the IS variability is known to organize the variability in the synoptic scale in a way that the amplitude of the synoptic

events change according to the IS phase (e.g., Liebmann et al. 1994, 2004), the IS variability could therefore also influence the initiation and evolution of convection (i.e. CSSWE).

Carvalho et al. (2002) is to our knowledge one of the few studies which linked the IS variability with mesoscale phenomena. In this case, the large-scale intraseasonal variability (10-70 days) in low-level wind regimes and mesoscale convective activity in tropical South America (north of 20°S) were related. They found that the contrasting IS low-level wind regimes are related to the phase of a dipole of large-scale OLR anomalies in tropical South America, which led to the study of the regional impacts of convective systems according to the phase of the wind regimes. Characteristics such as the number of convective systems, diurnal distribution, radius and fragmentation of the convective systems vary according to the IS wind regime (Carvalho et al. 2002).

However, the influence of the IS variability on the frequency and intensity of strong winds associated with deep moist convection has not been documented in Northeastern Argentina (NEA) region. Moreover, although several studies have analyzed the influence of IS variability on rainfall events over SESA either during the warm season (Nogues-Paegle and Mo, 1997, Liebmann et al. 1999, Gonzalez et al. 2008, Rickenbach et al. 2013, Gonzalez and Vera, 2014) or in the cold season (May to September, Alvarez, 2014), such influence during the transitional seasons (i.e., fall and spring) has not received similar attention yet. Previous studies have shown that during spring the interaction between baroclinic systems and strong moisture advection provides the

favorable environmental conditions for the development of severe weather events over SESA (Matsudo and Salio, 2011 and Mezher et al. 2012).

This paper seeks to advance in the understanding of the influence and modulation of the IS variability in NEA on the strong wind events associated with deep moist convection during spring season (SON, September, October and November). In order to achieve that, Convection-associated Strong Surface Wind Events (CSSWE) are defined and detected, and their modulation by the IS variability is then analyzed. The paper is organized as follows: section 2 describes the data and methodology used to detect the CSSWE events and to describe the IS variability in northeastern Argentina. Section 3 presents the main characteristics of the CSSWE events, their relationship with the activity of the leading pattern of IS variability and the dynamical conditions associated with CSSWE are discussed. Finally, conclusions and discussion are summarized in section 4.

2. Data and Methodology

2.1. Data

Hourly 10 m wind data and hourly Present Weather data from 9 surface stations of the National Weather Service in NEA (fig. 1) are used to detect CSSWE. The data used are presented in UTC time for a period of 14 years spanning from January 1st 1999 to December 31st 2012. The selected period of study used here was based on the availability of hourly surface station data.

To describe environmental variables, the Climate Forecast System Reanalysis (CFSR) NCEP database (Saha et al. 2010) is used. This database has a 0.5° resolution in latitude and longitude, 40 vertical levels and a temporal resolution of 6 hours. To complete the time series (from March 30th 2011 to December 31st 2012), CFS in its version 2 (CFSv2, Saha et al. 2014) with same temporal and spatial resolution is used. Daily data of interpolated OLR is taken from the National Oceanic and Atmospheric Administration (NOAA) database (Liebmann and Smith, 1996), with a 1º resolution and between 1999 and 2012 to perform composites and with a 2.5º resolution between 1980 and 2012 to compute the leading pattern of IS variability in South America.

2.2. Methodology

CSSWE are defined when the following criteria are all fulfilled:

(i) the intensity of the wind at 10 meters exceeds the spring-75th percentile for the given station,

(ii) at the time when (i) is observed, or within the 6 previous hours, the Present Weather code informed by the observer and recorded in the station is associated with convection. Those codes are 17 (thunderstorm, but no precipitation at the time of observation), 18 (squalls), and 80 to 99, which are related to showery precipitation or precipitation with current or recent thunderstorm, leaving out codes 83 to 86 as those are related to snow showers, which do not occur in NEA. This second criteria is adopted given that precipitation observations are not normally recorded hourly, but usually by a

6 or 24-hour accumulated period. Hourly Present Weather codes therefore guarantee the presence of convection at the moment of the strong wind observation.

If at least one hourly measurement that meets (i) and (ii) have been registered within a day, then that day is considered as a CSSWE day. The start day of the CSSWE is defined as "day 0". If the following day meets (i) and (ii) then the event is of 2 consecutive days (day 0 and day +1) and the same criteria for longer CSSWE. Following these criteria, CSSWE are determined in the period of study and then grouped into the following categories according with their duration: isolated events (i.e., CSSWE are registered only within one day, so they only have day 0), events lasting two consecutive days (day 0 and day +1) and events of three or more consecutive days. Once the CSSWE days have been obtained, the daily mean of the variables of the surface weather stations was computed and calculations are carried out with a daily framework.

The leading pattern of IS variability in eastern South America is considered, and hereafter called SIS (**S**eason-**I**ntra**S**easonal) pattern (Vera et al. 2017). Following the methodology proposed by Alvarez et al. (2014), an empirical orthogonal function (EOF) analysis is applied to the 1980-2012 spring daily OLR anomalies filtered on the 10-90-day band. The resulting leading EOF, hereafter as the spring-SIS pattern, is characterized by the spatial structure presented in Figure 2. The spring-SIS pattern presents a dipole, with one center of action extended over Paraguay and southern Brazil and another one located equatorward, where the SACZ variability maximizes and

explains 17.4% of the variance. The associated standardized principal component is used as an index to monitor the spring-SIS pattern activity. Its sign is defined such that a positive index value, which hereafter indicates a "positive phase" of the spring-SIS pattern, reflects favorable conditions for convection in SESA region and unfavorable conditions for convection in the SACZ, while a negative index value reflects favorable conditions for convection in the SACZ region and unfavorable conditions for convection in the SESA. The SIS index for the spring seasons between 1999 and 2012 was used to represent the IS variability within each season.

The evolution of the spring-SIS index is then related to the occurrence of CSSWE in NEA region. Those days in which the spring-SIS index resulted positive and exceeded one standard deviation are defined as a wet phase of the IS pattern. In this phase, OLR anomalies in the IS scale are negative over SESA region and then convection (and eventually, rainfall) is favored. Contrarily, those days in which the SIS index was negative and smaller than minus one standard deviation are defined as a dry phase, in which positive IS OLR anomalies occur in SESA and therefore inhibit rainfall conditions. The days previous to a wet or a dry phase of the SIS index were also objectively defined as categories pre-wet and pre-dry, as is explained below. The classification of the CSSWE is determined according to the day 0 of their occurrence: if day 0 occurred in a wet or dry phase of the spring-SIS pattern, the CSSWE is classified as wet or dry respectively. If day 0 occurred while the index was higher than one standard deviation but within the next 7 days it achieved a wet phase, then the CSSWE

is classified as pre-wet and if the index was in module lower than one standard deviation but within the next 7 days it achieved a dry phase, then the CSSWE is classified as pre-dry

This classification is not exhaustive, as the main focus is to relate the CSSWE with the development and occurrence of the phases of the spring-SIS pattern. Events which fall outside these four categories will be grouped in the neutral SIS category.

For anomalies calculation, the annual cycle was computed by smoothing the climatological daily means with a 31-point moving average and afterwards subtracted for each variable. A Lanczos bandpass filter of 63 weights (Duchon et al. 1979) is applied to the anomalies to obtain the 10-90-day filtered anomalies. Composites of filtered anomalies are computed according to the classification of the CSSWE events with respect to the spring-SIS index phase in which they occurred. The composites significance is tested through a local t-student test with a 95% confidence level for each grid point and level

3. Results

In the following subsections we analyze the IS modulation of CSSWE and the environmental IS dynamical conditions that favor their occurrence during austral spring. However, we first present a brief analysis on the seasonal distribution of CSSWE in order to identify the particularities of the SON season. The CSSWE distribution for each season is presented in table 1. A total of 715 events (31.1% of the total number of

days classified as CSSWE) are found during summer, similar to the number of events found during spring, 701 (30.5%). On the other hand, the number of events in winter and fall are 525 (22.8%) and 358 (15.6%) respectively. A CSSWE classification was also performed by clustering the CSSWE into the three categories (defined in section 2.2) according to their duration (table 1). For all three categories considered, the larger frequencies of occurrence are observed during summer and spring, while fewer total events are observed during winter and autumn. Isolated CSSWE occur more often during summer, while events of 2 or more days during the spring. This could be explained by that fact that during this particular season, the interaction between baroclinic systems and the strong moisture transport provides (i.e. strong low-level winds) a favorable environment to initiate a large number of deep convective events in middle and subtropical latitudes of SESA (Siqueira et al. 2004, Salio et al. 2007, Anabor et al. 2008 and Rasmussen et al. 2016). Therefore, this work seeks to improve the understanding of these spring events and the influence of the IS on them.

3.1. Intraseasonal modulation of CSSWE

Consecutive days of sustained low-level winds in the NEA region may be related to large-scale intraseasonal variations that exhibit an influence in the circulation patterns in South America, as the spring-SIS pattern or the MJO. The spectral distribution of variance of 10 m wind velocity daily mean compositions, obtained from the surface stations is analyzed, along with the averaged OLR for the reference box [31.5 ºS to 23.5 ºS and 61.5 ºW to 55.5 ºW] (figure 3). Surface (10 m) wind velocity shows spectral

peaks exceeding the red noise background spectrum at periods of 33, 19, and 17 days. The meridional component also shows significant peaks at 21, 12, and 10 days, while the zonal component seems to have no peaks in the IS scale (figures not shown). Likewise, the OLR variance spectrum also shows significant spectral peaks in the IS range, though at longer periods of: 40, 34, and 26 days. The IS time scale has therefore an influence in the variability of 10 m winds and also in convection over the study region. By representing the latter result with the activity of the spring-SIS pattern, the modulation over the CSSWE is studied.

In the following sections, only CSSWE that lasted at least 2 days will be considered, as they may be probably associated with more organized and durable systems, and therefore more easily modulated or influenced by the IS variability.

The different "flavours" in which IS variability can develop and its impact on the occurrence of CSSWE can be distinguished at a glance by observing the evolution of the spring-SIS index together with the occurrence of CSSWE. Figure 4 shows the percentage of stations that recorded a CSSWE for each day and the spring-SIS index value throughout the springs of 1999-2012. As seen in Figure 4, IS oscillations of the SIS index are not periodic -a wet phase is not always followed by a dry phase after some days- (e.g., compare in Fig. 4 springs of 2003 which is relatively periodic with 2009), nor wet and dry phases span an approximately same number of days (e.g. 2009 in Fig. 4). Also, it can be noted that CSSWE are more frequent prior to and during the wet phases of the spring-SIS index, while during the dry phases they are seldom seen.

For instance, between September 26th and September 29th 2004, a CSSWE of 4 days was observed, and in its day 0 the SIS index was of 0,28. As on days +2 and +3 the index was above 1 standard deviations, then this CSSWE is classified as a pre-wet case. This wet phase was followed by a dry phase in which no CSSWE were detected and then, during the wet phase of the index, between October 12th and October 13th a 2 days CSSWE was observed in 66.6% of the weather stations in NEA. As the SIS index in those days was greater than 1, the CSSWE is classified as a wet event. The spring of 2009 also showed some particularities: a persistent dry phase (9 days of the SIS index below -1) followed by a November of almost all days in a wet phase, during which long CSSWE were registered.

The modulation on CSSWE is now quantified by categorizing the occurrence of spring CSSWE according to the spring-SIS index evolution, as defined in section 2.2, and results are shown in table 2. In this way, we seek to identify if CSSWE are more frequent when the SIS index achieves a wet phase, during the days before it, when the index reflects a dry phase or before that stage. Most of the 2-day-long CSSWE are observed in the pre-wet phase (66) and in the wet phase (48), while the pre-dry and dry phases only present 16 and 24 cases respectively. The CSSWE that lasted 3 or more days were also more frequently observed during the wet (36) and pre-wet phases (28) of the index. It is particularly notable the scarce occurrence of CSSWE of 3 or more days in the dry and pre-dry phase of spring-SIS pattern, as they only represent 6.8% of the cases observed. Indeed, only 3 CSSWE of 3 days or more occurred in the dry phase of

the SIS index, which can be identified in Figure 4: between November 13th and November 17th 2005, a CSSWE of 5 days during which the SIS index started in a dry phase for 3 days and turned to a wet phase on days +5 to +7; between November 3th and November 7th 2009, a CSSWE of 5 days in which day 0 was the only one with a SIS index below -1 and then reaching a wet phase on days +5 to +7; and from September 19th to September 23rd of 2010, also of 5 days in which day 0 was the only one with a SIS index below -1 and then reaching a wet phase on days +4 to +6. Therefore, this long-lasting CSSWE, even though they were classified as occurring during a dry phase following our definition, do not seem to be associated exclusively to a dry phase of the SIS pattern but to a transition towards a wet phase.

Furthermore, from table 2 it follows that 69.9% of the CSSWE occur previous to, or during a wet/dry phase of the SIS index, while only 30.1% of the events are not related to the activity of this mode of variability (neutral SIS). Discarding those and therefore considering only the CSSWE that could be linked to IS variability, 79.1% of them occur before or during a wet phase of the index. For further analysis, spring CSSWE events of 2 and 3 or more consecutive days will be merged into one group.

To examine the evolution of the spring-SIS pattern according to the occurrence of CSSWE, an ensemble of the daily spring-SIS index values was calculated from day -6 to day +3 with respect to the start date (day 0) of the CSSWE. The median, first and third quartiles, and the 5th, 10th, 90th, and 95th percentiles of the spring-SIS index ensemble were calculated and presented in a box-plots form (Figure 5). The evolution of

the SIS index when a CSSWE occurred in day 0 in a pre-wet phase (Figure 5a) reveals a mean growth in the index since day -3. From day 0 onwards, the mean value of the index is positive and since day +2 is higher than one standard deviation, reflecting a wet phase of the index. The index dispersion, considering the 5^{th} and 95^{th} percentiles, is markedly reduced between days -2 and +3 compared to the previous days, and in more than 75% of the cases the index is positive on day +1, 95% on day +2 and all cases on day +3. The spring-SIS evolution for those CSSWE which started in a wet phase (Figure 5b) shows mean positive values since day -5, and at least in 95% of the cases the SIS index is positive between day -2 and +2, being on average greater than one standard deviation. The maximum value of the SIS index is reached, on average, on the second day of the CSSWE.

In the dry phase (fig. 5d), mean negative spring-SIS index values below one standard deviation are observed between days -3 and 0, reaching a minimum at day -1. In the pre-dry phase category (fig. 5c) no mean values, neither positive nor negative, exceeding one standard deviation of the spring-SIS index are observed. The average SIS index turns negative on day +2, however given the few cases in this category, results should be analyzed with caution.

3.2. Characterization of the environmental conditions of CSSWE associated with IS activity

In the previous section we have shown that the occurrence of CSSWE is modulated by the IS time scale, and particularly seen through the activity of the SIS pattern. Using 10-

90 filtered anomalies composites of CSSWE, we now analyze the large-scale IS circulation under which they are produced, taking into account the spring-SIS phase in which they occurred.

The IS-filtered 250-hPa geopotential height anomalies composites for the CSSWE days 0 are presented in Figure 6. Those CSSWE that were detected within a pre-wet phase (Fig. 6a) are related to a Rossby wave train arching in the South Pacific Ocean and towards South America. This wave shows an intense, statistically significant anticyclonic anomaly in the SE Pacific Ocean extending south to 75ºS and a cyclonic anomaly downstream, with a NW-SE orientation in the southern tip of South America. Also, an anticyclonic anomaly is located over the SESA region. Differently, when the CSSWE were registered during a wet phase of the SIS index, the wavetrain is seen to reflect more to the north, the anticyclonic anomaly is weaker and the cyclonic anomaly over South America is located farther northeast, with a more intense positive anomaly downstream (Fig. 6b). These type of wave trains have been often referred as Pacific-South American (PSA)-type teleconnections, after the work of Mo and Higgins (1998) and Mo and Paegle (2001).

Similar Rossby wave trains have been detected by Vera et al. (2017) related to the IS variability in South America. The authors analyzed separately the 30-90-day and 10-30-day IS variability, thereby separating the influence of the MJO and other sources of higher frequency in the IS time scale. Particularly, the wave trains found in Figs. 6a and 6b are similar to those associated with the evolution of an annual 10-30-days SIS

pattern during the SON trimester, the pre-wet cases to the days when the SIS phase changes towards a positive phase and the wet phase to the SIS positive phase (see Fig. 6 from Vera et al. 2017). Therefore, and also supported by Fig. 3a, it is the high-frequency IS variability which might modulate more clearly the occurrence of CSSWE.

Composites of the IS-filtered 250-hPa geopotential height anomalies associated with CSSWE events that were detected during a pre-dry phase (Fig. 6c) are not conclusive given the lack of statistical significance, again probably due to the low number of events in this category (Table 2). On the other hand, those CSSWE detected in a dry phase (Fig. 6d) are similar to the SIS negative phase regressions of Vera et al. (2017), though the subtropical wavetrain the authors observed in the western Pacific Ocean is not observed in Fig 6d. A positive geopotential height anomaly extends across central Argentina towards the South Atlantic Ocean, and significant cyclonic anomalies are observed both, upstream and downstream. Also, a strong cyclonic anomaly is located to the southeast of New Zealand as a part of these subpolar wavetrain (Fig. 6d).

Complementarily, Figure 7 presents the IS-filtered 850-hPa geopotential height anomalies composites for the CSSWE days 0. The low-level circulation composites show that the anomalies are approximately barotropic in the Pacific Ocean and are slightly ahead respect to upper-levels over South America. In both, pre-wet and wet composites (Figs. 7a, b), a cyclonic anomaly is observed over Argentina, favoring northerly and northwesterly wind into the NEA region where we identify the CSSWE. The strong anticyclonic anomaly upstream in the southeastern Pacific is observed in

both cases, farther to the north in the wet case (Fig. 7b). Differently, the low-level IS circulation when CSSWE are detected during a dry phase of the SIS index show an anticyclonic anomaly over the southwestern Atlantic Ocean, favoring easterly low-level winds which turn to be northerly over the NEA region (Fig. 7d). Low level conditions for moisture and heat transport are given for CSSWE in the dry phase, but NEA is affected by anticyclonic conditions, which inhibit the ascent, and it should be rarer to find convective cases.

The 10-90-day filtered OLR anomalies composites for the CSSWE days 0 are presented in Figure 8. The regional pattern in South America for those CSSWE that occurred during the wet phase is a dipole similar to the SIS pattern, as expected because of the methodology (Fig. 8b), as well as the regional pattern for the pre-wet cases (Fig. 8a), when the SIS pattern is building up. These maps again resemble those presented in Vera et al. (2017) for the 10-30-day IS variability of South American OLR anomalies for the positive and the change of phase respectively (see their Figure 5). It is also interesting that the weak tropical anomalies observed in the Indian Ocean for the CSSWE cases also match with the 10-30-day variability, and they do not match in sign with the 30-90-day variability (see Figure 2 of Vera et al. 2017), which is mainly related to the MJO. This might indicate that the MJO is not the primary cause of the wave trains, as it is not clearly seen in the composites. However, in particular cases the MJO influence may be more important or may even impact the 10-30-day variability by triggering other mechanisms. The composites of CSSWE days that occurred within a dry phase of the

SIS index (Fig. 8d) also show the regional pattern expected (a negative phase of the SIS pattern) and no other strong signal in the tropics.

Throughout this section we have showed that CSSWE are modulated by the regional IS variability through the SIS pattern, being the events favored mainly during the pre-wet and wet phases of the pattern. The composites of upper-level circulation and regional OLR anomalies have shown the IS conditions that create the environment which favors the development of convective strong winds events. However, there are still a small number of cases which occur when the IS modulation would not be favorable to develop in such conditions. Those cases might be explained by synoptic and/or meso scale activity, strong enough to cancel the IS inhibition and still produce a CSSWE.

4. Summary and Discussion

In this work we have detected the occurrence of strong surface wind events associated with convection (CSSWE) during austral spring in Northeastern Argentina and related it to the activity of the leading pattern of intraseasonal activity of OLR anomalies in South America, the SIS pattern. The variability of the SIS pattern follows the IS variability of precipitation, as previous studies have shown (Gonzalez et al. 2008, Alvarez et al. 2014). Moreover, studies have also confirmed that the IS evolution as described by the SIS index is not a purely regional phenomena, but it is instead related to the evolution of Rossby wave trains along the Pacific Ocean which eventually alter the regional circulation (e.g. Nogues-Paegle and Mo, 1997; Vera et al. 2017). These wave trains may be excited by convective activity in the tropics (as the MJO, the SPCZ) or by

sources of instability as the upper level jet stream activity (e.g., Trenberth 1986). The spring season was chosen as it was the season with largest amount of CSSWE detected of two or more consecutive days. The wind velocity taken from the surface stations in NEA showed significant peaks of activity revealing that the IS time scale, and especially the submonthly time scale, might be modulating the regional circulation that favors or not the occurrence of CSSWE.

The CSSWE were categorized according to the phase of the spring-SIS pattern. When considering those events related to SIS activity, almost 80% of them occurred before or during a wet phase, especially for the longer CSSWE. Furthermore, the detection of CSSWE days during and before a dry phase was scarce.

The evolution of the SIS index for the period that encompasses the CSSWE showed that those events detected before a wet phase were associated with a positive index from day 0 onwards and evolving to a spring-SIS index higher than one standard deviation on the next days (that is, the beginning of the period of CSSWE days is observed on average two days before the onset of the wet phase). When the CSSWE days begin in a wet phase of the index, positive values of the index were observed since day -5 and the SIS index remains greater than one standard deviation for 4 days (between day -2 and +2).

The hemispheric upper-level and regional low-level IS circulation that favors the development of CSSWE was also analyzed. At 250 hPa, PSA-like Rossby wave trains were observed to organize the circulation on IS time scales. When the CSSWE occur in a pre-wet phase, a strong anticyclonic anomaly in the SE Pacific Ocean and a cyclonic

anomaly in the southern tip of South America with a NW-SE orientation are observed. On the other hand, when the CSSWE are registered during a wet phase of the SIS index, on average the wave train is seen to refract farther the north, the anticyclonic anomaly is weaker and the cyclonic anomaly over South America is located more to the northeast. The persistence of the upper-level cyclonic anomaly in South America, favored by the IS variability, in roughly the same location for several days dynamically favors mid-level ascents in the region. Along with the northerly advection of humid air in the lower levels by the IS cyclonic anomaly over northern Argentina, this circulation sets the environment that promotes the development of CSSWE in the meso scale.

These Rossby wave trains are similar to those found by Vera et al. (2017) related to the IS variability in South America, and particularly to that in the 10-30-day time scale during the change of phase of the SIS index (from a dry to a wet phase) and during a wet phase. Also, the composites of IS-OLR anomalies result similar to those maps found by Vera et al. (2017) for the 10-30-day time scale, which together with the spectra of wind velocity previously mentioned, all support the conclusion that it is the higher-frequency IS variability the one which results more influential to the development of CSSWE. However, we do not out rule the influence of the MJO in particular cases. .

Finally, even though some CSSWE were detected on days with neutral SIS activity or even on a dry phase of the SIS index, which at least would not favor (from the IS time scale) the conditions for the development of convection in NEA, those events might be

generated exclusively by processes associated with the meso scale. Nonetheless, the association of most CSSWE days with a growing or a high SIS index found in this work is of great importance when studies of the predictability of the SIS index are being undertaken.

Acknowledgements

This study was supported by PICT 2008-215, PICT 2013-1299, PICT 2017- UBACyT 2013-2016- 20020130100618BA and UBACyT 2014-2017 20020130100618BA grants.

References

Alvarez, M. S., Vera, C. S., Kiladis, G. N. and Liebmann, B. (2016). Influence of the Madden Julian Oscillation on precipitation and surface air temperature in South America. Climate Dynamics, 46(1), 245-262, DOI 10.1007/s00382-015-2581-6

Alvarez, M. S., C. S. Vera, G. N. Kiladis and Liebmann, B. (2014). Intraseasonal Variability in South America during the Cold Season. Climate Dynamics. 42, 3253-3269, DOI 10.1007/s00382-013-1872-z

Anabor, V., Stensrud, D. J. and de Moraes, O. L. (2008). Serial upstream-propagating mesoscale convective system events over southeastern South America. *Monthly Weather Review*, *136*(8), 3087-3105.doi: http://dx.doi.org/10.1175/2007MWR2334.1

Berbery, E. H. and Barros, V. R. (2002). The hydrologic cycle of the La Plata basin in South America. *Journal of* Hydrometeorology, *3*(6).

Duchon, C. E. (1979). Lanczos filtering in one and two dimensions. *Journal of applied meteorology*, *18*(8), 1016-1022.

Carvalho, L. M., Jones, C. and Liebmann, B. (2004). The South Atlantic convergence zone: Intensity, form, persistence, and relationships with intraseasonal to interannual activity and extreme rainfall. *Journal of Climate*, *17*(1), 88-108.

Carvalho, L., Jones, C., & Silva Dias, M. A. (2002). Intraseasonal large - scale circulations and mesoscale convective activity in tropical South America during the TRMM -LBA campaign. *Journal of Geophysical Research: Atmospheres*, *107*(D20).

Gonzalez, P. L. and Vera, C. S. (2014). Summer precipitation variability over South America on long and short intraseasonal timescales. *Climate Dynamics*,*43*(7-8), 1993-2007.

González, P. L. M., Vera, C. S., Liebmann, B. and Kiladis, G. (2008). Intraseasonal variability in subtropical South America as depicted by precipitation data. *Climate dynamics*, *30*(7-8), 727-744.

Hirata, F. E. and Grimm, A. M. (2016). The role of synoptic and intraseasonal anomalies in the life cycle of summer rainfall extremes over South America. *Climate Dynamics*, *46*(9-10), 3041-3055.

Liebmann, B., Kiladis, G. N., Vera, C. S., Saulo, A. C. and Carvalho, L. M. (2004). Subseasonal variations of rainfall in South America in the vicinity of the low-level jet east of the Andes and comparison to those in the South Atlantic convergence zone. *Journal of Climate*, *17*(19), 3829-3842.

Liebmann, B., Kiladis, G. N., Marengo, J., Ambrizzi, T. and Glick, J. D. (1999). Submonthly convective variability over South America and the South Atlantic convergence zone. *Journal of Climate*, *12*(7), 1877-1891.

Liebmann B. and C.A. Smith, (1996). Description of a Complete (Interpolated) Outgoing Longwave Radiation Dataset. *Bulletin of the American Meteorological Society*, 77, 1275-1277.

Liu, C. (2011). Rainfall contributions from precipitation systems with different sizes, convective intensities, and durations over the tropics and subtropics. *Journal of Hydrometeorology*, *12*(3), 394-412.

Madden, R. A., and P. R. Julian (1994). Observations of the 40–50 day tropical oscillation: A review, *Mon. Weather Rev.*, 112, 814–837.

Marengo, J., W. R. Soares, C. Saulo and M. Nicolini. (2004). Climatology of the Low-Level Jet East of the Andes as Derived from the NCEP–NCAR Reanalyses: Characteristics and Temporal Variability. Journal of Climate. Vol. 17, No. 12, pp. 2261–2280.

Marengo, J. A., M. W. Douglas, and P. L. Silva Dias, (2002). The South American low level jet east of the Andes during the TRMM and LBA-WET AMC campaign. Journal of Geophysical Research: Atmospheres (1984–2012), 107(D20), LBA-47.

Matsudo, C. M. and Salio, P. V. (2010). Severe weather reports and proximity to deep convection over Northern Argentina. *Atmospheric Research*, *100*(4), 523-537.

Mezher, R. N., Doyle, M. and Barros, V. (2012). Climatology of hail in Argentina. *Atmospheric research*, *114*, 70-82.

Mo, K. C., & Paegle, J. N. (2001). The Pacific–South American modes and their downstream effects. *International Journal of Climatology: A Journal of the Royal Meteorological Society*, *21*(10), 1211-1229.

Mo, K. C., & Higgins, R. W. (1998). The Pacific–South American modes and tropical convection during the Southern Hemisphere winter. *Monthly Weather Review*, *126*(6), 1581-1596.

Nesbitt, S. W. and Zipser, E. J. (2003). The diurnal cycle of rainfall and convective intensity according to three years of TRMM measurements. *Journal of Climate*, *16*(10), 1456-1475.

Nogués-Paegle, J. and Mo, K. C. (1997). Alternating wet and dry conditions over South America during summer. *Monthly Weather Review*, *125*(2), 279-291.

Rasmussen, K. L., and R. A. Houze, Jr. (2016). Convective initiation near the Andes in subtropical South America. Mon. Wea. Rev., 144, 2351–2374.

Rasmussen, K. L., M. D. Zuluaga, and R. A. Houze, Jr. (2014). Severe convection and lightning in subtropical South America. *Geophys. Res. Lett.*, 41, 7359–7366, doi: 10.1002/2014GL061767.

Rickenbach, T. M., Nieto -Ferreira, R., B

Seasonal and regional differences in the rainfall and intensity of isolated convection over South America. *International Journal of Climatology*, *33*(8), 2002-2007.

Saha, S., Moorthi, S., Pan, H. L., Wu, X., Wang, J., Nadiga, S. and Iredell, M. (2010). The NCEP climate forecast system reanalysis. *Bulletin of the American Meteorological Society*, *91*(8).

Saha, S., Moorthi, S., Wu, X., Wang, J., Nadiga, S., Tripp, P., ... & Ek, M. (2014). The NCEP climate forecast system version 2. *Journal of Climate*, *27*(6), 2185-2208.

Salio, P., Nicolini, M. and Zipser, E. J. (2007). Mesoscale convective systems over southeastern South America and their relationship with the South American low-level jet. *Monthly Weather Review*, *135*(4), 1290-1309.

Silva Dias, M. A. F. (1999). Storms in Brazil. *Hazards and Disasters Series—Storms,* R.

Pielke Sr. and R. Pielke Jr., Eds., Vol. II, Routledge, 207–219.

Siqueira, J. R. and Toledo Machado, L. A. (2004). Influence of the frontal systems on the day-to-day convection variability over South America. *Journal of Climate*, *17*(9), 1754-1766.

Trenberth, K. E. (1986). An assessment of the impact of transient eddies on the zonal flow during a blocking episode using localized Eliassen-Palm flux diagnostics. *Journal of the Atmospheric Sciences*, *43*(19), 2070-2087.

Vera, C., Baez, J., Douglas, M., Emmanuel, C. B., Marengo, J., Meitin, J. and Zipser, E. (2006). The South American low-level jet experiment. *Bulletin of the American Meteorological Society*, *87*(1), 63-77.

Vera, C.S., Alvarez, M.S., Gonzalez, P.L.M., Liebmann B., Kiladis G.N. (2017). Clim Dyn. https://doi.org/10.1007/s00382-017-3994-1

Zipser, E. J., Liu, C., Cecil, D. J., Nesbitt, S. W. and Yorty, D. P. (2006). Where are the most intense thunderstorms on Earth? *Bulletin of the American Meteorological Society*, *87*(8), 1057-1071.

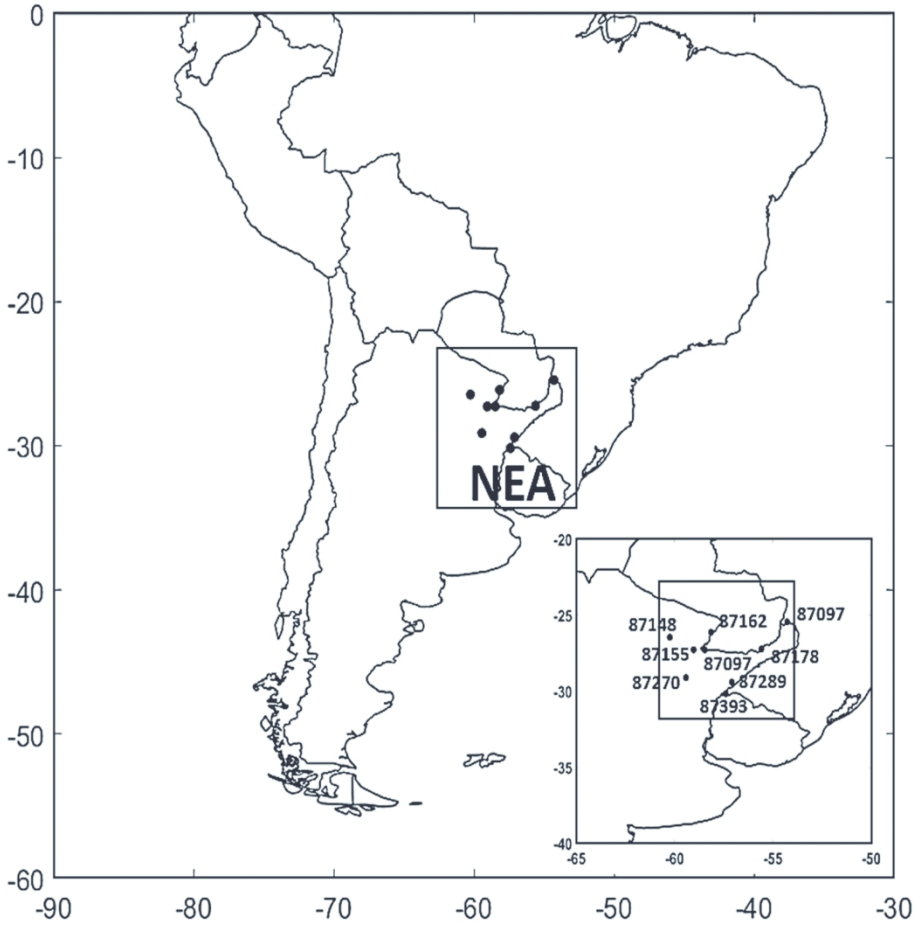

Figure 1: South America map and surface station (dot). Rectangle denotes Northeastern Argentine region (NEA). Zoom over the study area with surface station number (bottom right). The inner area corresponds to the region from which OLR was averaged to compute the spectrum.

150x150mm (300 x 300 DPI)

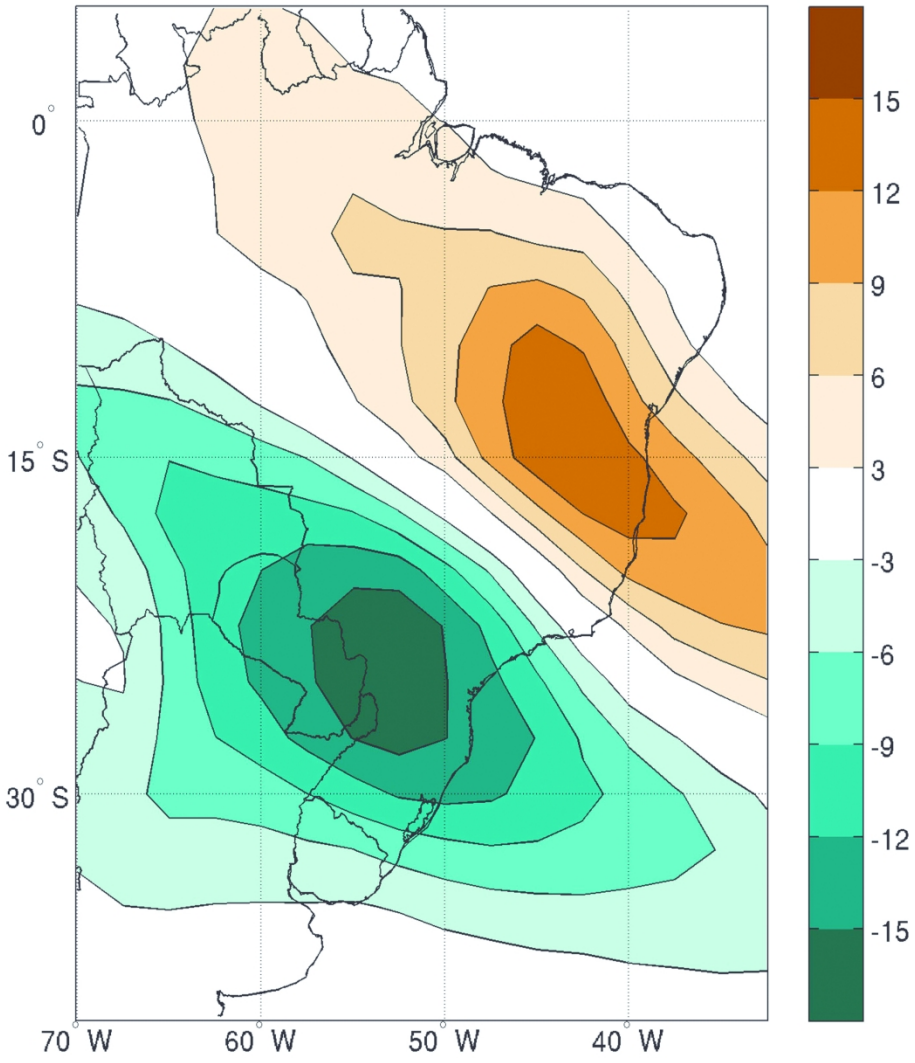

Figure 2: First leading Empirical Orthogonal Function (EOF) of FOLR for the spring season (spring-SIS pattern). Contour interval is 3 and 0 contour is omitted. Units are in Wm-2.

260x320mm (300 x 300 DPI)

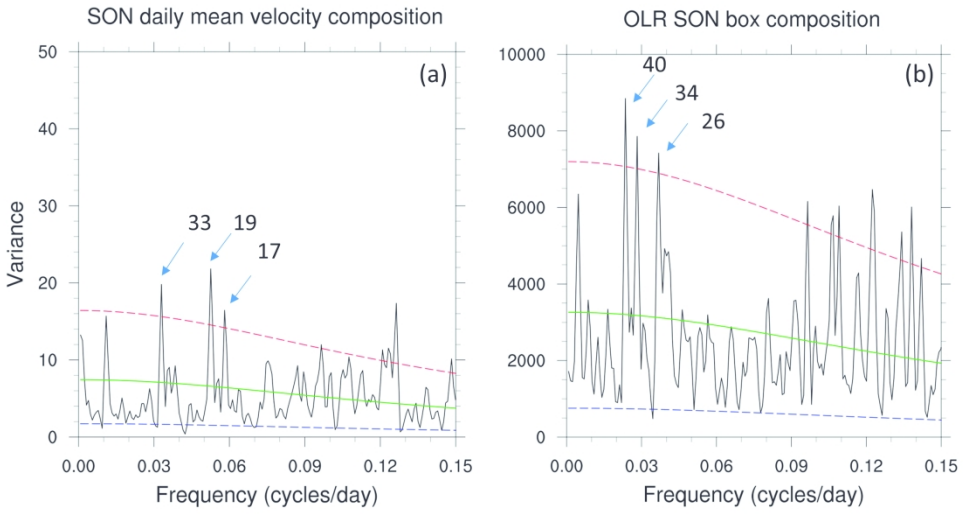

Figure 3: Power spectrum of daily mean 10 m wind velocity in $(ms^{-1})^2$ and b) daily mean OLR $(Wm^{-2})^2$ for the reference box. The dashed lines indicated in each spectrum are the red noise background spectrum and 95% confidence level, respectively. The main spectral peaks (in days) are shown inside each spectrum.

239x150mm (300 x 300 DPI)

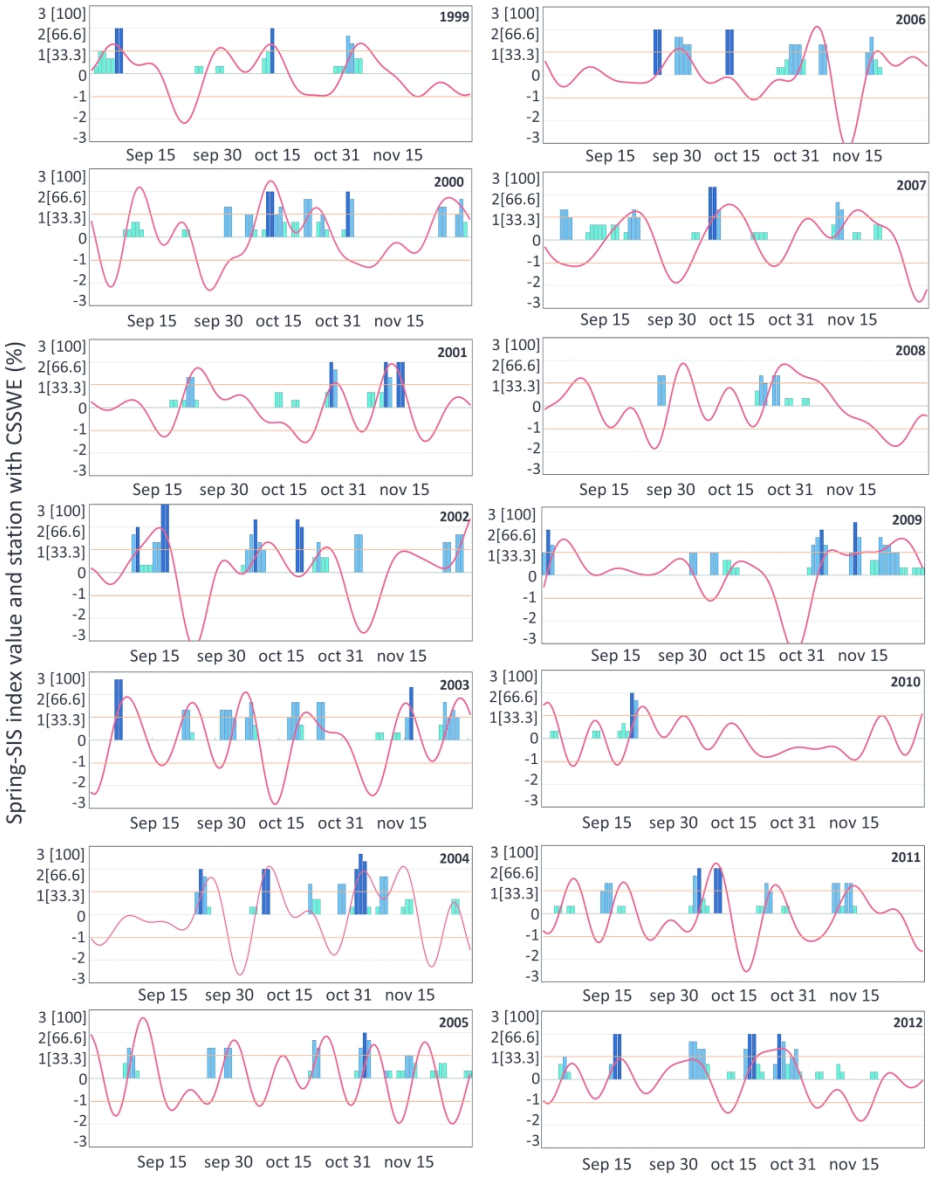

Figure 4: Temporal evolution of the spring-SIS index (red solid line) with the percentage of stations with CSSWE (blue bars) for the spring 1999-2012. The one-standard deviation threshold is marked as reference. Light blue bar corresponds to a less than 33% of station with CSSWE, medium blue to those between 33-66% and dark blue higher than 66%.

260x320mm (300 x 300 DPI)

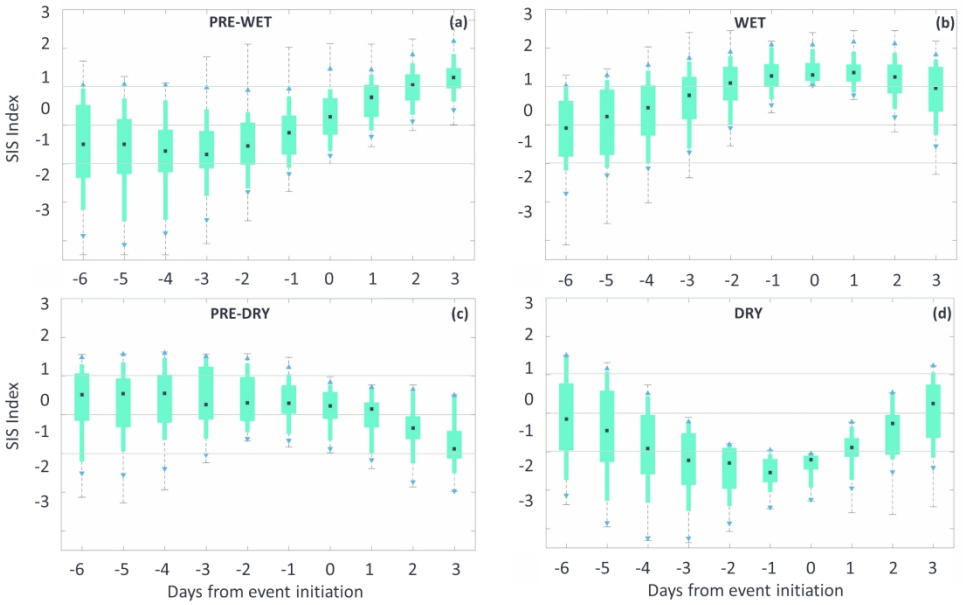

Figure 5: Mean spring-SIS evolution and box plot associated with CSSWE for each spring-SIS index phases from day -6 to +3. a) pre-wet, b) wet, c) pre-dry and d) dry. Events start on day 0. The center mark of each box represents the median, coarser box are the 25th and 75th percentiles, finer box are the 10th and 90th percentiles, arrows are the 5th and 95th percentiles and whiskers extend to the extreme values, below and above the 5th and 95th percentiles respectively. One standard deviation with light gray line.

239x150mm (300 x 300 DPI)

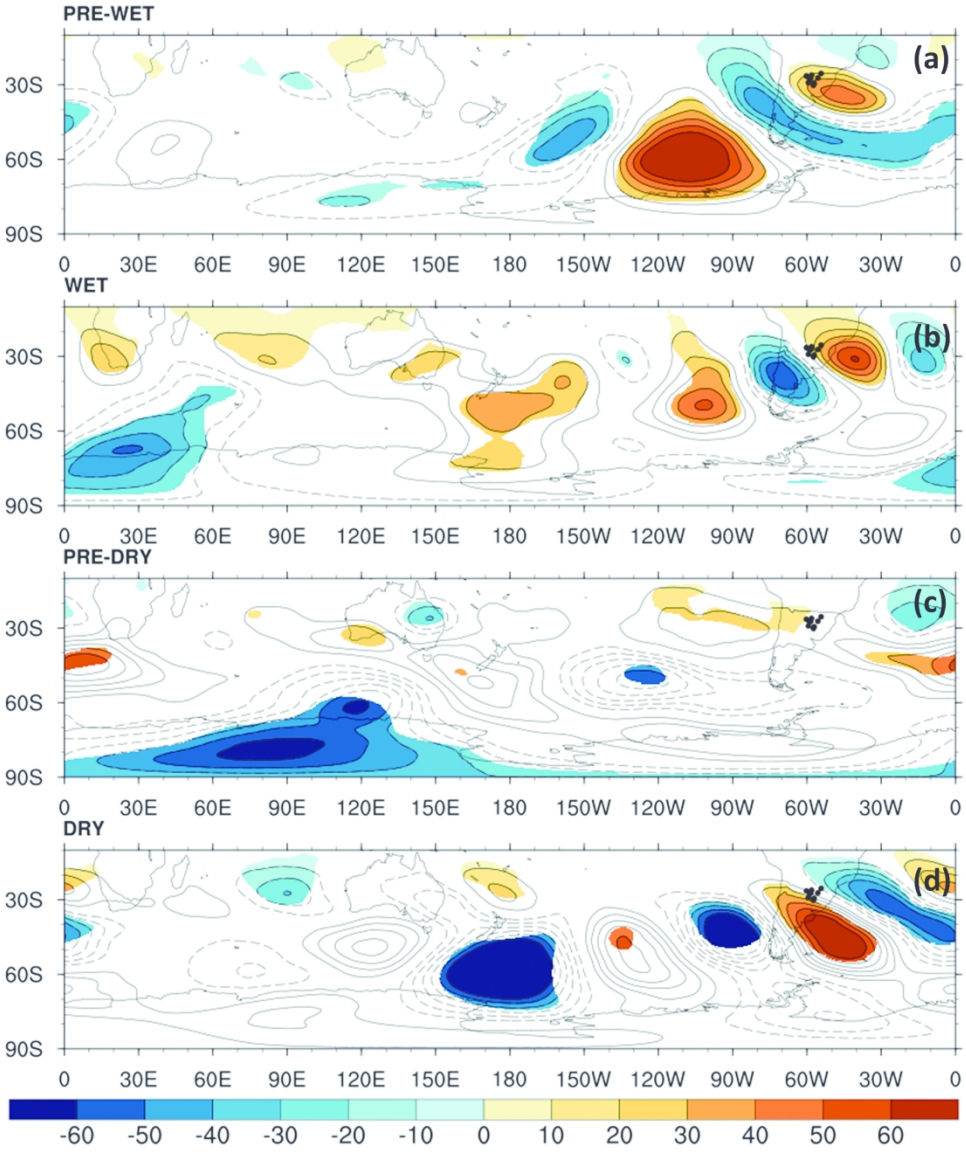

Figure 6: Filtered 10-90 days geopotential height anomalies composites at 250 hPa [gpm] for each spring-SIS phase. a) pre-wet, b) wet, c) pre-dry and d) dry. Positive anomalies are presented in solid line and negative values are dashed. 95% significant values of the composition are shaded. Surface stations are indicated by black dots.

170x199mm (300 x 300 DPI)

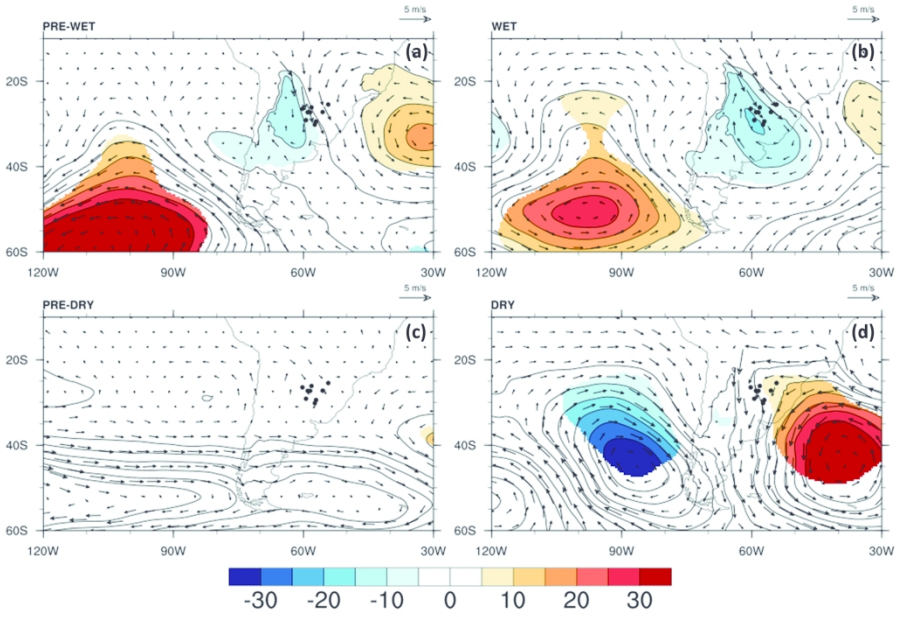

Figure 7: Filtered 10-90 days geopotential height anomalies composites at 850 hPa [gpm] and wind anomalies [ms^{-1}] for each spring-SIS phase. a) pre-wet, b) wet, c) pre-dry and d) dry. Positive anomalies are presented in solid line and negative values are dashed. 95% significant values of the composition are shaded. Surface stations are indicated by black dots.

239x150mm (300 x 300 DPI)

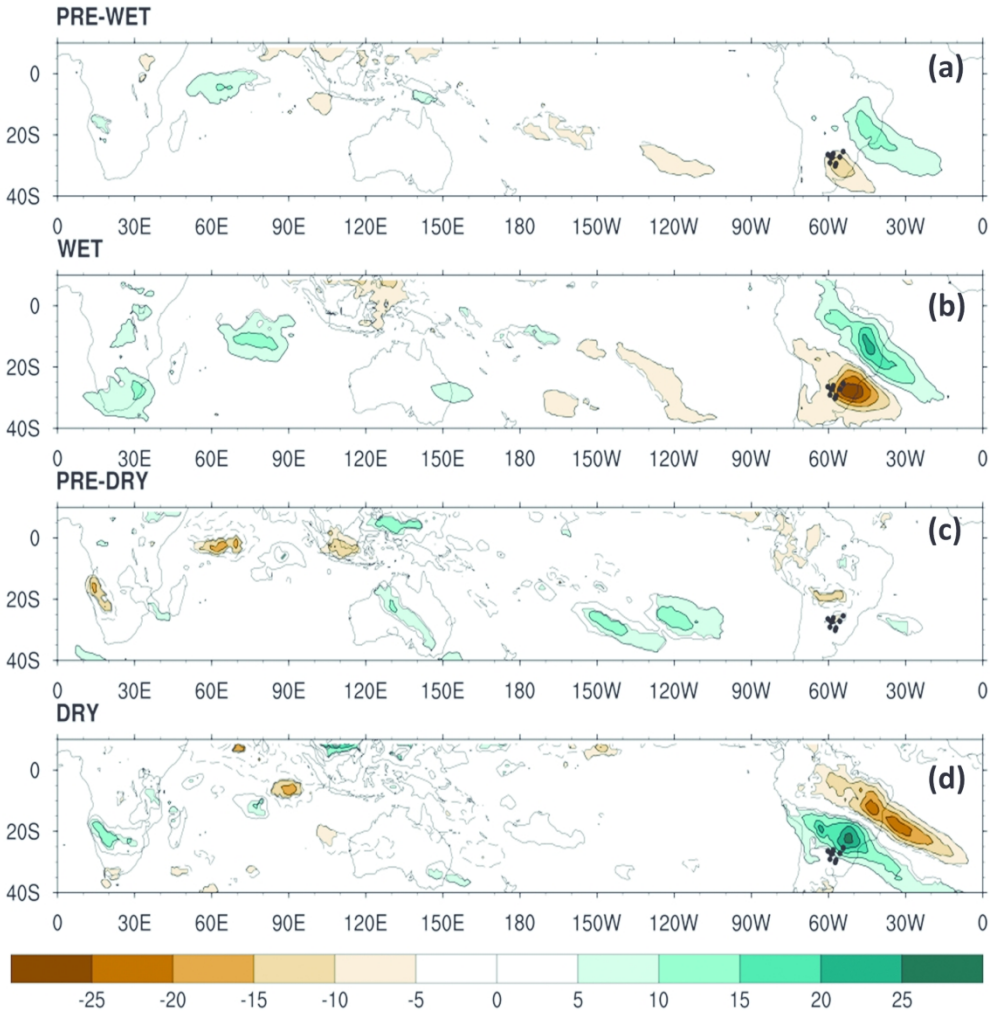

Figure 8: Filtered OLR anomalies [Wm^{-2}] for each spring-SIS phase. a) pre-wet, b) wet, c) pre-dry and d) dry. 95% significant values of the composition are shaded. Surface stations are indicated by black dots.

170x199mm (300 x 300 DPI)

	1 day	2 days	≥3 days	Total events
Spring (SON)	379 (54.0%)	219 (31.2%)	103 (14.7%)	701 (30.5%)
Summer (DJF)	438 (61.2%)	204 (28.5%)	73 (10.2%)	715 (31.1%)
Fall (MAM)	333 (63.4%)	152 (28.9%)	40 (7.6%)	525 (22.8%)
Winter (JJA)	224 (61.5%)	107 (29.9%)	27 (7.5%)	358 (15.6%)
Total	1374 (59.8%)	682 (29.6%)	243 (10.6%)	2299 (100%)

Table. 1. Number of CSSWE for each of the three categories according to their duration and for the four seasons of the year. Also shown are, for each season, the percentage of events that lasted 1, 2 or 3 or more days. Last column shows the amount of the total events per season and the percentage respect to the yearly total. Last row shows the amount and percentage in each of the three categories.

	Pre-Wet	Wet	Pre-Dry	Dry	neutral SIS	Total
2 Days	66 (30.1%)	48 (21.9%)	16 (7.3%)	24 (10.9%)	65 (29.7%)	219 (68%)
≥ 3Days	28 (27.2%)	36 (34.9%)	4 (3.9%)	3 (2.9%)	32 (31.1%)	103 (32%)
Total	94 (29.2%)	84 (26.1%)	20 (6.2%)	27 (8.4%)	97 (30.1%)	322 (100%)

Table 2. Number of spring CSSWE of 2 days and 3 or more days for each category defined based on spring-SIS index phases (pre-wet, wet, pre-dry, dry and neutral SIS). See Section 2.2 for details.